Wall turbulence at high friction Reynolds numbers

Sergio Hoyas [1,*] Martin Oberlack [2,3] Francisco Alcántara-Ávila [1]
Stefanie V. Kraheberger,[2,3] and Jonathan Laux[2]

[1]*Instituto Universitario de Matemática Pura y Aplicada, Universitat Politècnica de València, Camino de Vera, 46024 València, Spain*
[2]*Technical University of Darmstadt, Chair of Fluid Dynamics, Otto-Bernd-Straße 2, 64287 Darmstadt, Germany*
[3]*Technical University of Darmstadt, Centre for Computational Engineering, Dolivostrasse 15, 64293 Darmstadt, Germany*

A new direct numerical simulation of a Poiseuille channel flow has been conducted for a friction Reynolds number of 10 000, using the pseudospectral code LISO. The mean streamwise velocity presents a long logarithmic layer, extending from 400 to 2500 wall units, longer than it was thought. The maximum of the intensity of the streamwise velocity increases with the Reynolds number, as expected. Also, the elusive second maximum of this intensity has not appeared yet. In case it exists, its location will be around $y^+ \approx 120$, for a friction Reynolds number extrapolated to approximately 13 500. The small differences in the near-wall gradient of this intensity for several Reynolds numbers are related to the scaling failure of the dissipation, confirming this hypothesis. The scaling of the turbulent budgets in the center of the channel is almost perfect above 1000 wall units. Finally, the peak of the pressure intensity grows with the Reynolds number and does not scale in wall units. If the pressure at the wall is modeled as an inverse quadratic power of Re_τ, then $p'^+_\infty \approx 4.7$ at the limit of infinite Reynolds number.

I. INTRODUCTION

After almost 140 years of the publication of Reynolds's first work [1], turbulence is still an open problem. As wall-bounded turbulence is responsible for up to 5% of the CO_2 dumped by humanity every year [2], this challenge is of special importance. Research of turbulent flows has been dominated by experimental techniques until the 1980s, where supercomputers started to be powerful enough to solve the equations of turbulent flows. Direct numerical simulation (DNS), where almost all scales are simulated, is the only reliable technique to study turbulence. However, due to the highly nonlinear behavior of wall-turbulent flows, DNS are restricted to simplified geometries, with one or two periodic directions. The most studied of these idealized flows are Poiseuille turbulent channels, see Fig. 1, where the fluid is confined between two parallel plates and the flow is driven by pressure.

The friction Reynolds number, defined as $\mathrm{Re}_\tau = u_\tau h/\nu$, is the main control parameter in wall-bounded turbulence. Here $u_\tau = \sqrt{\tau_w/\rho}$ is the friction velocity, ν is the kinematic viscosity, ρ is the
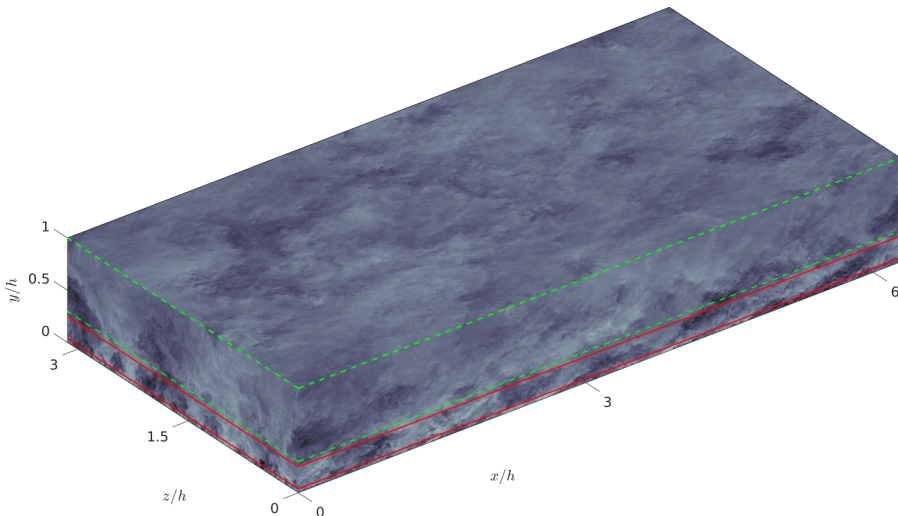
---

*serhocal@mot.upv.es

FIG. 1. Lines as in Table I. (a) Instantaneous streamwise velocity perturbation, arbitrary units. The flow goes from the left to the right. Only the bottom part of the channel is shown. Red lines: log layer. Green lines, outer region.

density, and τ_w is the friction at the wall. h is the semiheight of the channel and is equivalent to the radius in pipes and δ_{99} in boundary layers. Since the seminal work of Kim, Moin, and Moser [3], the Re_τ has steadily increased from 180 in 1987 to 8000 in 2018 [3–9]. A simulation reaching the $\text{Re}_\tau = 10\,000$ frontier is presented here. This friction Reynolds number is less than the largest realization of the flow obtained by experimental means; see Ref. [10] and discussion inside. In particular, Ref. [10] reaches a value of $20\,000$ with a very good spatial resolution. However, the main advantage is that DNS allows one to compute any imaginable quantity in the whole domain, including derivatives close to the wall. Apart from contributing to the discussion of several questions that have arisen in the last years, with this simulation we provide the community data with the hope of contributing to better modeling of turbulence.

A companion paper of this work is Ref. [11]. That paper deals with the confirmation of the Lie-symmetry-based theory of turbulence or more precisely the derivation of arbitrary moment scaling laws for the log and the deficit region of the flow. In the present article we will restrict ourselves to present the data and the kinematics of the flow, referring the interested reader to that article for scaling laws about the streamwise mean velocity. This work is organized as follows. Section II describes the numerical method and the validation of the data. Section III discusses the one-point statistics of the flow, including mean flow and intensities. The energy turbulent budgets are discussed in Sec. IV. Finally, Sec. V contains the conclusions of this work.

II. NUMERICAL METHOD

In this work we present the results of a DNS of a pressure-driven (Poiseuille) channel flow (see Fig. 1) at a nominal $\text{Re}_\tau = 10\,000$. Superscript $(+)$ indicates that the quantities have been normalized by u_τ and ν. This simulation has been performed in a computational box of sizes $L_x = 2\pi h$, $L_y = 2h$ and $L_z = \pi h$. This box is large enough to accurately describe the statistics of the flow [12,13]. The streamwise, wall-normal, and spanwise coordinates are x, y, and z, respectively. The corresponding velocity components are U, V, and W or, using index notation, U_i. Statistically averaged quantities in time, x and z are denoted by an overbar, $\overline{U}$, whereas fluctuating quantities are denoted by lowercase letters, i.e., $U = \overline{U} + u$. Primes are reserved for intensities, $u' = \overline{uu}^{1/2}$.

TABLE I. Parameters of the simulations. Re_b is the bulk Reynolds number, $\mathrm{Re}_b = U_b h/\nu$, where U_b is the bulk velocity. Δ_x^+ and Δ_z^+ are in terms of dealiased Fourier modes. The last column is the total simulation time without transition in terms of eddy turnovers.

Case	Line	Re_τ	Re_b	L_x	L_z	Δx^+	Δz^+	Tu_τ/h
HJ02	......	2000	43 650	$8\pi h$	$3\pi h$	12.3	6.1	11
LJ04	- - - -	4000	98 302	$2\pi h$	πh	12.8	6.4	15
LM05	— ·	5200	125 000	$8\pi h$	$3\pi h$	8.2	4.1	7.80
HO10	——	10 000	261 000	$2\pi h$	πh	15.3	7.6	19.8

The flow can be described by means of the mass balance and momentum equations,

$$\partial_j U_j = 0, \tag{1}$$

$$\partial_t U_i + U_j \partial_j U_i = -\partial_i P + \frac{1}{\mathrm{Re}_\tau} \partial_{jj} U_i, \tag{2}$$

where repeated subscripts indicate summation over 1,2,3 and the pressure term includes the density. These equations have been solved using the LISO code, which has successfully been employed to run some of the largest simulations of turbulence [6,14–17]. Briefly, the code uses the same strategy as Ref. [3], but using a seven-point compact finite difference in the y direction with fourth-order consistency and extended spectral-like resolution [18]. The temporal discretization is a third-order semi-implicit Runge-Kutta scheme [19]. The wall-normal grid spacing is adjusted to keep the resolution at $\Delta y = 1.5\eta$, i.e., approximately constant in terms of the local isotropic Kolmogorov scale $\eta = (\nu^3/\epsilon)^{1/4}$. In wall units, Δy^+ varies from 0.3 at the wall, up to $\Delta y^+ \simeq 12$ at the centerline. The resolution in x and z is similar to the largest simulations of turbulence; see Table I. A code similar to the one used presently, including the energy equation, is explained in Ref. [20].

The initial file of this simulation was taken from a smaller Reynolds number simulation. To accelerate the compilation of statistics, three initial files were prepared and thus three simulations were run at the same time. In every case, the code was run until some transition phase had passed and the flow had adjusted to the new set of parameters. Once the flow was in a statistically steady state, statistics were compiled. The running times to compile statistics are shown in terms of eddy-turnovers in the rightmost column of Table I. The transitions until the simulations reached a statistically steady state, which were very time consuming, are not contemplated in this table.

Table I also shows the parameters of the simulations HJ02 [6], LJ04 [12], and LM05 [8]. These simulations will be used in the paper in the color code described in the second column of Table I. As it is said above, this code has already proved its worth, but to further validate the statistics, Fig. 2(a) shows the error in the momentum equation,

$$\frac{d\overline{U}^+}{dy^+} - \overline{uv}^+ = 1 - y^+.$$

The difference between both sides of this equation is below 2×10^{-3}, similar to the other three simulations utilized here. Thus, it has been considered that enough statistical information was obtained. The details about the size of the box has been given earlier, but to stress the validity of the box, the spectral energy densities for u and v, $\phi = k_x k_z E(k_x, k_z)$, at $y^+ \approx 15$, the peak of u', are given in Fig. 2(b). Here, $\lambda = 2\pi/k$. All the significant scales are captured in the computational box. This further confirms that the large and wide structures at the right corner are inactive in the sense of Townsend [6,21,22]. They are present in u spectra but neither in v or uv cospectra. More details about the spectra will be given in a forthcoming manuscript. Finally, to further post-process the simulation a total of 300 temporal images of the velocity field have been stored, with a size of roughly 90TB. This database is open to the community under a reasonable request.
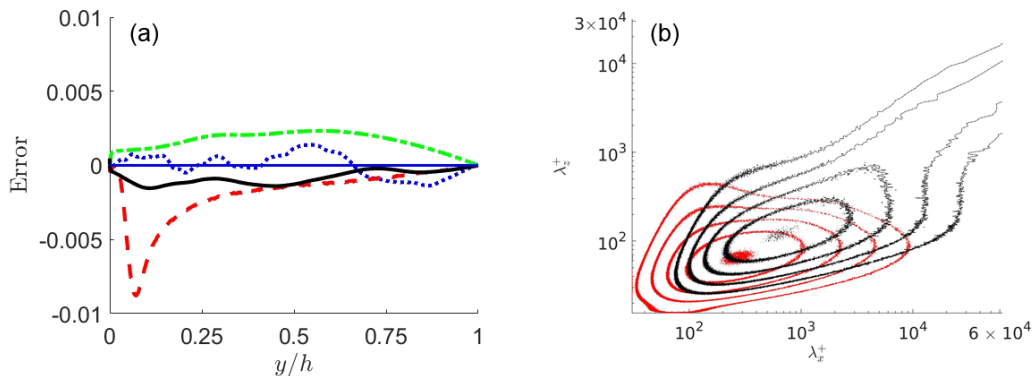
FIG. 2. Lines as in Table I. (a) Error in the computation of momentum equation. (b) 2D power spectra at $y \approx 15$. U (black) and V (red). The inner isolines represents 90% of the maximum energy. From there, each isoline is half of the energy of the previous one.

III. ONE-POINT STATISTICS

The mean velocity profile is shown in Fig. 3(a) in terms of the indicator function, $\Gamma = y^+ \partial_{y^+} \overline{U}^+$. This function should show a plateau if the classical scaling for the logarithmic layer $\overline{U}^+ = \kappa^{-1} \log(y^+) + B$ holds, where κ is the von Kármán constant. Moreover, in Ref. [11] it is shown that the profile of $\overline{U}^+$ is indeed logarithmic. For every case, the first local minimum of Γ is reached around $y^+ \approx 70$, which more or less coincide with the classic starting point of the logarithmic layer [23]. However, the indicator function is not flat until $y^+ \approx 400$, so this could be a new starting point. The logarithmic layer extends to around $y^+ \approx 2500$ or $y/h = 0.25$, above the usual value of $y/h = 0.2$. To obtain the values of κ and B, we have restricted ourselves to the region where the indicator function is flattest, i.e., from $y^+ = 400$ to $y/h = 0.25$ [Fig. 3(b)], obtaining $\kappa = 0.394$ and $B = 4.61$. More details about the selection of this interval are given in Ref. [11]. This value of κ is similar to the experimental one of [24], and only 0.010 and 0.007 units larger than the one given by Refs. [8,9]. Abe and Antonia [25] also obtained this value in their study of global energy. Studying the finite Reynolds number effects on the flow, Luchini [26], and Spalart and Abe
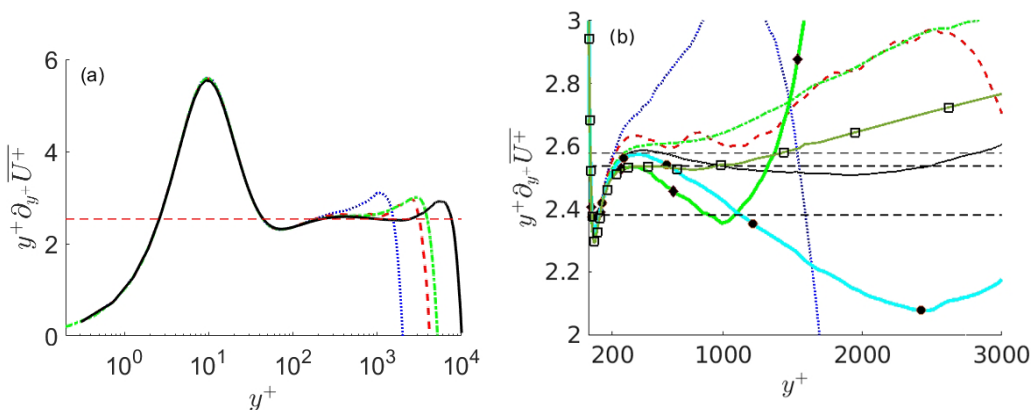

FIG. 3. Lines as in Table I. (a) Indicator function, showing a log layer in the range $y^+ = 400$–2500. (b) Zoom of the previous figures. Straight dashed lines: $\kappa = 0.388, 0.394$, and 0.42. Continuous lines: Spalart and Abe [27] LE functions for HO02 and LM05 (green, diamonds), and LM05 and HO10 (light blue, circles). Monkewitz [29] indicator function model (dark green, open squares)
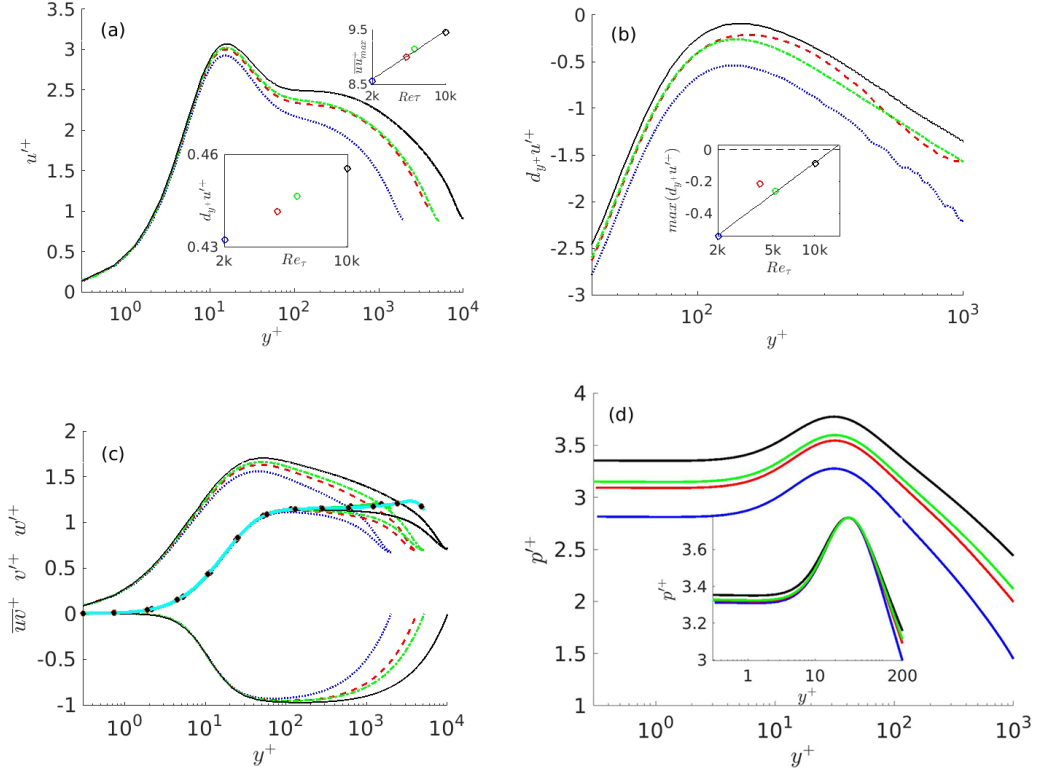
FIG. 4. Lines as in Table I. (a) u'^+. Box: $d_{y+}u'^+$ evaluated at the wall. (b) $d_{y+}u'^+$, close to the possible second maximum. Box: maximum value of $d_{y+}u'^+$ (c) v'^+, w'^+ and $\overline{uv}$. Continuous lines with circles: Spalart and Abe [27] LE functions for HO02 and LM05 (green), and LM05 and HO10 (light blue) for v'^+. (d) Intensity of total pressure. Box: shifting of all pressures to the peak of HO10 case.

[27], give a similar value. In this last work, an algorithm to compute the Luchini extrapolation for infinite Reynolds number is given. This approximation has been reproduced using the same data as Ref. [27], and the new data available, lines with circles of Fig. 3(b). This procedure, taking κ as the maximum of the curve, would lead to $\kappa = 0.388$, a bit smaller than the one given in Ref. [27].

It is worth mentioning that some other authors, with different tools, have obtained values above 0.40. McKeon [28] in high Reynolds numbers involving pipes got 0.42. More recently, Monkewitz [29] has developed an algorithm to model $\overline{U}^+$ for very large Reynolds numbers. The profile of the indicator function using this model is shown in Fig. 3(b). The value of κ is similar to the one obtained by us. However, in Ref. [29] the actual logarithmic profile for $Re_\tau = 10^5$ would start around 10^3 wall units for a final value $\kappa = 0.42$. As a DNS reaching this Re_τ is approximately 3500 times more costly than the one presented here, this is probably an open problem for the next decade or more.

The intensity of the streamwise velocity, u'^+, is shown in Fig. 4(a). The well-known scaling failure in the buffer layer is still present [6], and the maximum of the intensity is $u'^+ = 3.07$. Lee and Moser [8] found that this limit is growing in several DNS studies of canonical flows, in the range $Re_\tau = 1000$–5200. However, several experimental studies [30,31] suggested that this limit could be bounded. Following Ref. [32], the value of the first maximum seem to follow a logarithmic law, $\max \overline{uu}^+ \approx 0.55 \log Re_\tau + 4.4$ (Fig. 4(a), right corner). The value given in Ref. [33] is $\max \overline{uu}^+ \approx 0.63 \log Re_\tau + 3.8$, suggesting that the growing of the maximum in channels with respect to the Reynolds number is slower than in other wall-bounded flows. In a different approach, Chen and Sreenivasan [33] collected all the data available, showing that this maximum is indeed limited.

They fitted the data to different law, $\max \overline{uu}^+ \approx A - B\mathrm{Re}_\tau^{(-1/4)}$, obtaining a finite value for this peak at infinite Reynolds number. Similar to this work, this growing is related to the scaling failure of the dissipation [34], as it is shown later.

About the open question of a possible second maximum of u'^+ the situation is shown in Fig. 4(b). Notice that the existence of this second maximum could lead to the presence of new phenomena at the beginning of the logarithmic layer [35]. If it exists, then this maximum would be located around $y^+ \approx 120$. However, the derivative of u'^+ is still not zero. Fitting the data to a logarithmic grow law, we obtain $d_y u_0'^+ = 0.29 \log \mathrm{Re}_\tau - 2.7$, and a approximate critical value of $\mathrm{Re}_\tau = 13500$, which is a bit smaller than the one estimated in Ref. [10].

The other three remaining components of the Reynolds stress tensor can be seen in Fig. 4(c). As expected, the scaling of v'^+ and $\overline{uv}^+$ is almost perfect near the wall. v'^+ presents a large plateau in the log layer, but following Ref. [27], it is expected to grow for infinite Reynolds number [lines with circles, Fig. 4(c)]. In the case of w'^+ the maximum keeps growing, causing a minor scaling failure in the viscous sublayer. Pressure, Fig. 4(d), is computed as in Ref. [36], growing at the wall logarithmically [37,38]. The peak is at $y^+ \approx 30$ for all simulations. Even if the curves seems to be parallel, they are not. In the box of Fig. 4(d), where we have drifted HJ02, LJ04, and LM05 so they coincide in their maximum with HO10, it is appreciated than the scaling is not perfect either. The pressure at the boundary grows as $P_0 = 0.33 \log \mathrm{Re}_\tau + 0.30$ and $P_{\max} = 0.31 \log \mathrm{Re}_\tau + 0.96$. Notice that P_0 grows faster than $P_{\max}$. However, if this law applies, then they will not be equal until extremely high values of the Reynolds number. The data also fits extremely well to the law suggested in Ref. [33], $\max \overline{p}^+ \approx 4.78 - 10.002\mathrm{Re}_\tau^{(-1/4)}$. In this case, the limit value for the pressure would be $p_\infty^+ \approx 4.7$, but more points are needed at larger Reynolds number to test both laws.

IV. TURBULENT BUDGETS

The budget equation for the component $\overline{u_i u_j}$ of the Reynolds-stress tensor is written as [34,39]

$$B_{ij} \equiv D\overline{u_i u_j}/Dt = P_{ij} + \varepsilon_{ij} + T_{ij} + \Pi_{ij}^s + \Pi_{ij}^d + V_{ij}. \tag{3}$$

The terms in the right-hand side of Eq. (3) are referred as production, dissipation, turbulent diffusion, viscous diffusion, pressure-strain, and pressure-diffusion. They are defined by

$$P_{ij} = -\overline{u_i u_k}\partial_k \overline{U_j} - \overline{u_j u_k}\partial_k \overline{U_i}, \quad \varepsilon_{ij} = -2\nu\overline{\partial_k u_i \partial_k u_j},$$
$$T_{ij} = \partial_k \overline{u_i u_j u_k}, \quad V_{ij} = \nu \partial_{kk}\overline{u_i u_j},$$
$$\Pi_{ij}^s = \overline{p(\partial_j u_i + \partial_j u_i)}, \quad \Pi_{ij}^d = \partial_k(\overline{pu_i}\delta_{jk} + \overline{pu_j}\delta_{ik}), \tag{4}$$

where δ_{ij} is Kronecker's δ. The splitting of the pressure in two different terms is not unique, but this one offers more information in the B_{12} and B_{22} terms [34]. Finally, in channels $B_{ij} \equiv 0$.

In the viscous and buffer layers, budgets should scale in wall units, $B_{ij}^+ = B_{ij}\nu/u_\tau^3$. The budgets are shown in Fig. 5, using this scale. Except for those terms that are identically zero, all are active. The well-known scaling failure [34] of the dissipation at the wall for B_{11} is still present, Fig. 5(a). As expected, all terms collapse for $y^+ > 10$. However, below this more or less arbitrary limit, the absolute values of ε_{11}^+ and V_{11}^+ increase with the Reynolds number. This scaling failure can be linked to the growing of the first maximum of u'^+. At the wall [34],

$$V_{11}|_{y=0} = \nu \partial_{yy}\overline{u^2}|_{y=0} = 2\nu\overline{(\partial_y u)^2}|_{y=0} = -\varepsilon_{11}, \tag{5}$$

as all other terms vanish. Similarly to Refs. [17,40], u'^+ can be approximated by

$$u'^+ = (b_u y^+ + c_u y^{+2} + ...). \tag{6}$$

Therefore, near the wall, $u'^+ \approx b_u y^+$ and $V_{11}^+ \approx b_u^2$. Thus, the reason why this term of the turbulent budget does not scale with the Reynolds number in the wall comes from the differences in the b_u terms. This term represents the slope of u'^+ near the wall. Looking at the box in Fig. 4(a),
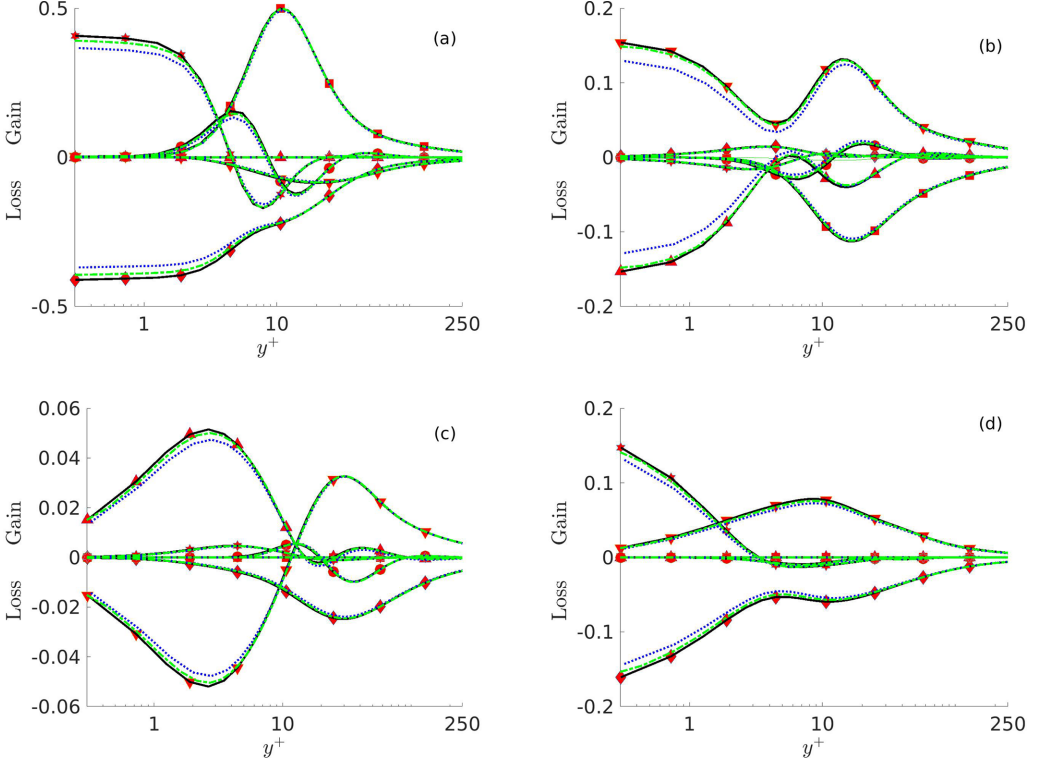
FIG. 5. Lines as in Table I. Budgets for Reynolds stresses in wall units. (a) B_{11}^+, (b) B_{12}^+, (c) B_{22}^+, (d) B_{33}^+. Production ■, dissipation ◆, viscous diffusion ∗, pressure-strain ▽, pressure diffusion ▲, turbulent diffusion •.

one can see that, effectively, the value of du'^+/dy^+ at the wall does not collapse, but it slightly increases. Apart from our data, there are evidences that the peak at $y^+ \approx 15$ keeps growing with respect to Re_τ [10]. Because the position of the peak is constant in y^+, the slope of u'^+ has to be higher for larger Re_τ. In other words, as long as the peak of u'^+ increases with Re_τ, b_u will also increase and V_{11}^+ cannot scale at the wall. In the case of passive thermal flows, the behavior of the thermal field is similar to the streamwise velocity. It was observed in Ref. [41], that in thermal flows for high Prandtl numbers the peak value of the temperature intensity, θ'^+, was approximately constant with respect to the Reynolds number. This yielded a constant value of the derivative of θ'^+ at the wall and, therefore, a much better scaling of the viscous diffusion term for the energy equation near the wall. A similar argument, but using production instead of dissipation, is shown in Ref. [33] highlighting this relationship.

The scaling failures of the pressure terms, Figs. 5(b) and 5(c), are harder to explain because there are no good models for them [34]. However, it seems that this scaling failure is decreasing with the Reynolds number, even if the pressure keeps growing at the wall, as it is shown in Fig. 4(d).

The situation in the center of the channel is better explained using a different adimensionalization, $B_{ij}^* = yB_{ij}/u_\tau^3$; see Fig. 6. This scaling counteracts the expected decay of these terms far from the wall, which is roughly as y^{-1}. To avoid numerical noise, the turbulent diffusion has been computed here using the fact that $B_{ij} \equiv 0$. Above $y/h \approx 0.2$ the scaling is almost perfect, but in the case of the production term of B_{11}^*. This scaling failure is linked to the unsuccessful scaling of u' with y/h in the outer region due to the effect of large scales [38]. Abe and Antonia [25] demonstrated that small scales are likely to lose the Reynolds-number dependence more rapidly than large scales given a more distinct overlap scaling for the dissipation than for the mean velocity, which explain
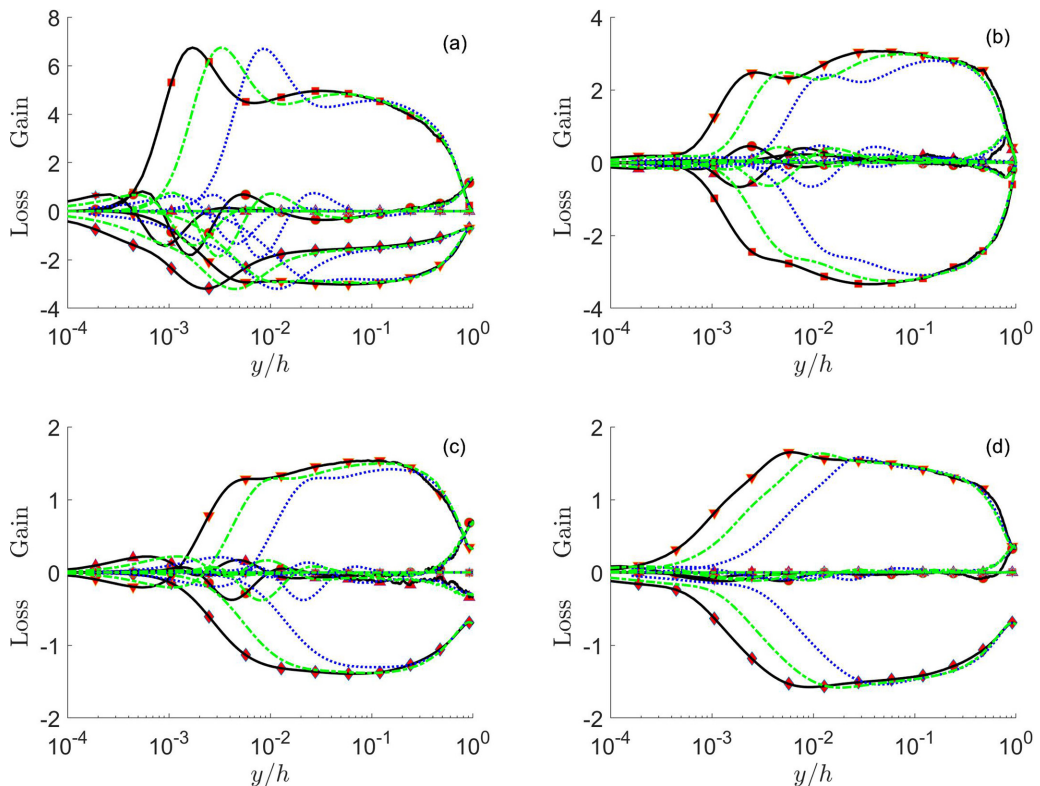
FIG. 6. Lines as in Table I. Premultiplied budgets for the different terms of the Reynolds stresses, $B_{ij}^* = yB_{ij}/u_\tau^3$. (a) B_{11}^*, (b) B_{12}^*, (c) B_{22}^*, (d) B_{33}^*. Production ■, dissipation ◆, viscous diffusion ∗, pressure-strain ▼, pressure diffusion ▲, turbulent diffusion ●.

this small scaling failure. In agreement with previous results [34,39] all the budgets above the buffer layer, $y/h \approx 10^{-3}$ in this case, are dominated by a few terms. The streamwise velocity fluctuations introduce the turbulent energy in the flow. This energy is dissipated by the dissipation and the pressure-strain terms Fig. 6(a). Notice that $P_{11} \approx 2\varepsilon_{11}$ and that in the channel center the turbulent diffusion becomes dominant in the production of energy, as U^+ flattens.

This energy is redistributed by pressure to $\overline{vv}$ and $\overline{ww}$, where it is basically dissipated by the dissipation, Figs. 6(c) and 6(d). Notice, however, that pressure diffusion plays an important role in the channel center. Finally, for the Reynolds stress $\overline{uv}$ Fig. 6(b) production and pressure strain are the dominant terms, but above $y/h \approx 0.5$ pressure diffusion and turbulent diffusion are also present.

V. CONCLUSIONS

To conclude, we have simulated a Poiseuille turbulent channel flow at a friction Reynolds number of $\text{Re}_\tau = 10\,000$. This simulation was made in a small box of size $(2\pi h, 2h, \pi h)$, large enough to accurately compute the statistics of the flow. The profile of $\overline{U}$ shows a long log layer, extending from $y^+ \approx 400$ to $y^+ \approx 2500$. The value of the von Kármán constant is $\kappa = 0.394$. The first maximum of the streamwise profile u'^+ continues growing, which is the cause of the scaling failure of the dissipation at the wall. The second maximum of u'^+ has not appeared yet, and it is foreseen to appear at approximately $\text{Re}_\tau = 13\,500$. However, the turbulent budgets show a almost perfect scaling in the outer region with $B_{ij}^* = yB_{ij}/u_\tau^3$. Two growing laws are presented for the pressure, predicting a value of $p_\infty^+ \approx 4.7$

A paper about new scaling laws using Lie-symmetry theories has been published together with this work [11], and some more results about the spectra and the dynamics of the flow will be published shortly.

The database containing the mean flow, intensities, and turbulent budgets can be downloaded from the TUdatalib Repository of TU Darmstadt at Ref. [42].

---

[1] O. Reynolds, An experimental investigation of the circumstances which determine whether the motion of water shall be direct or sinuous, and of the law of resistance in parallel channels, Proc. R. Soc. Lond. **174**, 935 (1883).

[2] J. Jiménez, Near-wall turbulence, Phys. Fluids **25**, 101302 (2013).

[3] J. Kim, P. Moin, and R. Moser, Turbulence statistics in fully developed channels flows at low Reynolds numbers, J. Fluid Mech. **177**, 133 (1987).

[4] R. Moser, J. Kim, and N. Mansour, Direct numerical simulation of turbulent channel flow up to $Re_\tau = 590$, Phys. Fluids **11**, 943 (1999).

[5] J. Del Alamo, J. Jiménez, P. Zandonade, and R. Moser, Scaling of the energy spectra of turbulent channels, J. Fluid Mech. **500**, 135 (2004).

[6] S. Hoyas and J. Jiménez, Scaling of the velocity fluctuations in turbulent channels up to $Re_\tau = 2003$, Phys. Fluids **18**, 011702 (2006).

[7] M. Bernardini, S. Pirozzoli, and P. Orlandi, Velocity statistics in turbulent channel flow up to $Re_\tau = 4000$, J. Fluid Mech. **758**, 327 (2014).

[8] M. Lee and R. Moser, Direct numerical simulation of turbulent channel flow up to $Re_\tau \approx 5200$, J. Fluid Mech. **774**, 395 (2015).

[9] Y. Yamamoto and Y. Tsuji, Numerical evidence of logarithmic regions in channel flow at $Re_\tau = 8000$, Phys. Rev. Fluids **3**, 012602(R) (2018).

[10] M. Samie, I. Marusic, N. Hutchins, M. Fu, Y. Fan, M. Hultmark, and A. Smits, Fully resolved measurements of turbulent boundary layer flows up to $Re_\tau = 20\,000$, J. Fluid Mech. **851**, 391 (2018).

[11] M. Oberlack, S. Hoyas, S. V. Kraheberger, F. Álcantara-Ávila, and J. Laux, Turbulence Statistics of Arbitrary Moments of Wall-Bounded Shear Flows: A Symmetry Approach, Phys. Rev. Lett. **128**, 024502 (2022).

[12] A. Lozano-Durán and J. Jiménez, Effect of the computational domain on direct simulations of turbulent channels up to $Re_\tau = 4200$, Phys. Fluids **26**, 011702 (2014).

[13] F. Lluesma-Rodríguez, S. Hoyas, and M. Peréz-Quiles, Influence of the computational domain on DNS of turbulent heat transfer up to $Re_\tau = 2000$ for Pr = 0.71, Int. J. Heat Mass Transf. **122**, 983 (2018).

[14] V. Avsarkisov, S. Hoyas, M. Oberlack, and J. García-Galache, Turbulent plane Couette flow at moderately high Reynolds number, J. Fluid Mech. **751**, R1 (2014).

[15] V. Avsarkisov, M. Oberlack, and S. Hoyas, New scaling laws for turbulent Poiseuille flow with wall transpiration, J. Fluid Mech. **746**, 99 (2014).

[16] S. Kraheberger, S. Hoyas, and M. Oberlack, DNS of a turbulent Couette flow at constant wall transpiration up to $Re_\tau = 1000$, J. Fluid Mech. **835**, 421 (2018).

[17] F. Alcántara-Ávila, S. Hoyas, and M. Pérez-Quiles, Direct numerical simulation of thermal channel flow for $Re_\tau = 5000$ and $Pr = 0.71$, J. Fluid Mech. **916**, A29 (2021).

[18] S. K. Lele, Compact finite difference schemes with spectral-like resolution, J. Comput. Phys. **103**, 16 (1992).

[19] P. R. Spalart, R. D. Moser, and M. M. Rogers, Spectral methods for the Navier-Stokes equations with one infinite and two periodic directions, J. Comput. Phys. **96**, 297 (1991).

[20] F. Lluesma-Rodríguez, F. Álcantara-Ávila, M. Pérez-Quiles, and S. Hoyas, A code for simulating heat transfer in turbulent channel flow, Mathematics **9**, 756 (2021).

[21] A. Townsend, *The Structure of Turbulent Shear Flows*, 2nd ed. (Cambridge University Press, New York, 1976).

[22] A. Lozano-Durán and H. J. Bae, Characteristic scales of Townsend's wall-attached eddies, J. Fluid Mech. **868**, 698 (2019).

[23] S. B. Pope, *Turbulent Flows* (Cambridge University Press, Cambridge, UK, 2000).

[24] I. Marusic, J. P. Monty, M. Hultmark, and A. J. Smits, On the logarithmic region in wall turbulence, J. Fluid Mech. **716**, R3 (2013).

[25] H. Abe and R. Anthony Antonia, Relationship between the energy dissipation function and the skin friction law in a turbulent channel flow, J. Fluid Mech. **798**, 140 (2016).

[26] P. Luchini, Universality of the Turbulent Velocity Profile, Phys. Rev. Lett. **118**, 224501 (2017).

[27] P. Spalart and H. Abe, Empirical scaling laws for wall-bounded turbulence deduced from direct numerical simulations, Phys. Rev. Fluids **6**, 044604 (2021).

[28] B. J. McKeon, J. Li, W. Jiang, J. F. Morrison, and A. J. Smits, Further observations on the mean velocity distribution in fully developed pipe flow, J. Fluid Mech. **501**, 135 (2004).

[29] P. Monkewitz, The late start of the mean velocity overlap log law at-a generic feature of turbulent wall layers in ducts, J. Fluid Mech. **910**, A45 (2021).

[30] M. Hultmark, M. Vallikivi, S. C. C. Bailey, and A. J. Smits, Turbulent Pipe Flow at Extreme Reynolds Numbers, Phys. Rev. Lett. **108**, 094501 (2012).

[31] C. E. Willert, J. Soria, M. Stanislas, J. Klinner, O. Amili, M. Eisfelder, C. Cuvier, G. Bellani, T. Fiorini, A. Talamelli *et al.*, Near-wall statistics of a turbulent pipe flow at shear Reynolds numbers up to 40 000, J. Fluid Mech. **826**, R5 (2017).

[32] I. Marusic, W. J. Baars, and N. Hutchins, Scaling of the streamwise turbulence intensity in the context of inner-outer interactions in wall turbulence, Phys. Rev. Fluids **2**, 100502 (2017).

[33] X. Chen and K. R. Sreenivasan, Reynolds number scaling of the peak turbulence intensity in wall flows, J. Fluid Mech. **908**, R3 (2021).

[34] S. Hoyas and J. Jiménez, Reynolds number effects on the Reynolds-stress budgets in turbulent channels, Phys. Fluids **20**, 101511 (2008).

[35] I. Marusic, B. J. Mckeon, P. A. Monkewitz, H. M. Nagib, A. J. Smits, and K. Sreenivasan, Wall-bounded turbulent flows at high Reynolds numbers: Recent advances and key issues, Phys. Fluids **20**, 065103 (2010).

[36] J. Kim, On the structure of pressure fluctuations in simulated turbulent channel flow, J. Fluid Mech. **205**, 421 (1989).

[37] J. Jiménez and R. D. Moser, What are we learning from simulating wall turbulence? Phil. Trans. R. Soc. Lond. A **365**, 715 (2007).

[38] J. Jiménez and S. Hoyas, Turbulent fluctuations above the buffer layer of wall-bounded flows, J. Fluid Mech. **611**, 215 (2008).

[39] N. N. Mansour, J. Kim, and P. Moin, Reynolds-stress and dissipation-rate budgets in a turbulent channel flow, J. Fluid Mech. **194**, 15 (1988).

[40] H. Kawamura, K. Ohsaka, H. Abe, and K. Yamamoto, DNS of turbulent heat transfer in channel flow with low to medium-high Prandtl number fluid, Int. J. Heat Fluid Flow **19**, 482 (1998).

[41] F. Alcántara-Ávila and S. Hoyas, Direct numerical simulation of thermal channel flow for medium-high Prandtl numbers up to $Re_\tau = 2000$, Int. J. Heat Mass Transf. **176**, 121412 (2021).

[42] M. Oberlack, S. Hoyas, F. Alcántara-vila, S. Kraheberger, and J. Laux, TUdatalib Repository, 2021, https://doi.org/10.48328/tudalib-658.